2-2020

Influence of Solvent and Molecular Weight in Wrinkle Formation in Spin-cast Polystyrene Thin Films

Chunyi Tang

Matthew Mullen

William B. Euler

AIMS Materials Science, 7(1): 60–74.
DOI: 10.3934/matersci.2020.1.60
Received: 26 November 2019
Accepted: 04 February 2020
Published: 20 February 2020

http://www.aimspress.com/journal/Materials

Research article

Influence of solvent and molecular weight in wrinkle formation in spin-cast polystyrene thin films

Chunyi Tang[1,2], Matthew Mullen[3] and William B. Euler[3,*]

[1] College of Biological and Chemical Engineering, Guangxi University of Science and Technology, No. 268 Donghuan Road, Chengzhong District, Liuzou, Guangxi, 545006, P. R. China
[2] Key Laboratory for Processing of Sugar Resources of Guangxi Higher Education Institutes, Guangxi University of Science and Technology, Liuzhou 545006, P. R. China
[3] Department of Chemistry, 140 Flagg Road, University of Rhode Island, Kingston, RI, 02881, USA

* **Correspondence:** Email: weuler@chm.uri.edu; Tel: +14018745090.

Abstract: The surface morphology of polystyrene thin films formed from various molecular weight polystyrene and solvent conditions is studied. When spin-cast from tetrahydrofuran (THF) wrinkles are formed at the extremities that have periodicity with wavelengths in the μm range and amplitudes in the nm range but varies with molecular weight. A mixed solvent system consisting of THF and dimethylformamide (DMF) leads to periodic structures only with THF-rich compositions. THF and DMF have similar properties relevant to spin-casting: density, surface tension, molecular weight, and viscosity but different boiling points and room temperature vapor pressures, demonstrating that formation periodicity requires a volatile solvent. The formation of the surface structures is attributed to the Marangoni effect and the film thicknesses and wave parameters are shown to be consistent with literature models.

Keywords: morphology; polymer; solvent casting; wrinkle formation; spin-coating

1. Introduction

In the present state of materials science, where there is a push for devices to be made smaller, it is important to understand a material's physical and chemical properties from both the perspective of the surface and the bulk. It is well documented that a material can behave differently when

comparing these two regions of the same substance [1–5], which is often attributed to confinement effects. Furthermore, an additional area becomes of importance when the surfaces of two different materials interact to form an interface. A defining feature of an interface is the surface morphology, which is a broad term and can be considered on many different scales. In modern thin film systems one must consider the nano/micrometer regions of surface morphology as well as the macro features. Changing and controlling surface morphology through the use of etching and lithography in hard materials such as silicon wafers has been well studied and understood for some time now [6–8]. However, polymers are playing a larger role in devices and new methods are needed to control surface morphology. The push for understanding and controlling surface morphologies historically arises from the field of adhesion [9,10], but certain patterning in materials has been shown to be promising for use in photonic devices [11–20], stretchable microelectronics [21,22], mechanically switchable wetting [23], and microfluidics [24,25]. Methods currently used for producing surface patterns in soft materials include thin film dewetting [26–28], electrohydrodynamic patterning [29,30], breath figures [31,32], thermal-gradient induced patterning [33,34], self-assembly and microphase separation [28,35,36] electron irradiation [37] but most commonly used is template based patterning [38–40]. Template based patterning can be used to create various different types of geometric structures such as hexagons, stripes, or rectangles, however the most common use of templating is the production of wrinkles (also known as striations or corrugations) on a surface [41–44]. To induce wrinkling on a surface, a layer of elastomer, typically polydimethylsiloxane (PDMS), is prestrained mechanically or thermally. A rigid skin layer is then transferred onto the elastomer and the strain is released, which causes buckling of the skin layer and produces wrinkles, creases, or folds.

Herein we report a simple spin casting method that can be used to fabricate polystyrene thin films that have different surface morphologies. Modification of the surface morphology of polymer films has long been studied with the goal of controlling the structure [45–52]. Wrinkles in the PS films form spontaneously without the use of PDMS, away from the center of the sample. The surface morphology, as determined by the wavelength and amplitude of the periodic structures, can be controlled by the spin-speed, solvent composition, and the polymer molecular weight but the solution concentration has minimal effect on these parameters. We find that a high evaporation rate is required to obtain a periodic surface morphology while a low evaporation rate leads to a random surface structure. This is consistent with previous studies showing the role of solvent evaporation of polymer solutions under non-spinning conditions [53].

The parameters required to understand spin-cast films have been studied for a long time [54,55] and are reasonably well understood. Several solvent properties influence the final film characteristics, including vapor pressure, density, and molecular weight. Standard spin-coating theory [54,55] predicts smooth films but with the observation of wrinkle formation during spin-coating [50,51,56] new theories were developed, primarily to understand how to prepare uniform films rather than create nanostructured surfaces [57–61]. Two different mechanism were proposed to explain the wrinkle formation. De Gennes [58] suggested that as evaporation occurred a thin layer of a glassy polymer formed on the surface that buckled upon final drying. In contrast, Birnie [60] developed a model based on the Marangoni effect, which arises from differential evaporation that induces a stress field that lead to disruptions that control the final surface structure. Birnie [60] determined that the surface morphology was controlled by the relative effects of evaporation rate and surface tension. Experimental work supports the Marangoni model [57,59,61–64] although there are still unanswered

questions [61]. Our results support the Birnie model [60] which adds sinusoidal perturbations to standard thickness models.

PS has been shown to show nonuniform and periodic surface morphologies when cast from single component good solvents [39,47,49]. We find that the wrinkle amplitude and wavelengths scale with the dry film thickness but are independent of the concentration of polymer when spin-cast from pure THF. In contrast, a solvent system composed of THF mixed with dimethylformamide (DMF), two solvents that have about the same molecular weight, density, and surface tension but drastically different vapor pressure, periodic structures are only found for THF-rich compositions. The role of solvent composition has not been reported previously.

2. Materials and methods

Glass (borosilicate) slides were cut into 3.75 × 1.75 cm pieces (2 mm thick). These were then cleaned first by sonication in 95% ethanol (EtOH, Pharmaco-Aaper) for 15 min, then by sonication in DI water for 15 min, and finally dried with N_2. Polystyrene (PS, Polymer Source Inc.) solutions were made in solvent (tetrahydrofuran (THF, Sigma Aldrich, HPLC Grade) or THF/dimethylformamide (DMF, Sigma Aldrich, HPLC Grade) mixtures. Each solution was sonicated for 4 h or until the entire polymer was dissolved. The PS films were made by spin-casting using fresh solutions. A 500 μL aliquot of the PS solution was deposited in the center of the glass substrate. Spin-casting was done at room temperature under a N_2 blanket (to remove humidity effects) with an acceleration of 1080 rad·s^{-2} for all solutions but different final rotation rates and spin times were used. To achieve different PS film thickness either the spin speed or the PS concentration was varied. After spinning, the films were placed in a 60 °C oven for 1 min to dry.

The film thickness of the PS was determined using a Filmetrics F40 microscope via reflection spectroscopy. The reflection spectrum was recorded with a tungsten-halogen light source over the range of 400–900 nm. The resulting interference pattern was then fit using the known refractive index of the polymer to give the average film thickness. After the film thickness was determined, the surface morphology of the PS films was analyzed using a Filmetrics Profilm 3D Optical Profiler. The images of the surface were obtained using either the vertical scanning interferometry (VSI) or phase shifting interferometry (PSI) modes. The evaporation rates of PS/DMF/THF solutions were measured by placing a 0.5 mL aliquot of solution on a glass substrate on a balance (23 °C, 20% humidity). The mass was recorded as a function of time until the mass leveled off.

3. Results and discussion

The spin coating method for fabricating thin films is often used because it is a simple method to create uniform films of a desired thickness. However, the actual dynamics of spin casting are complicated, as the final product and quality of the film depend on many factors. As Bornside et al. [55] have demonstrated, the final thickness of a dry film, h_o, can be estimated through the following equation,

$$h_o = \chi_{pol}^{o}\left[\eta_o\left(\frac{cD_g}{\nu_g^{1/2}\rho}\right)\left(\frac{p_{sol}M_{sol}}{RT}\right)\left(1-\chi_{pol}^{o}-\chi_{sol}^{\infty}\right)\right]^{1/3}\frac{1}{\omega^{1/2}} \quad (1)$$

where η_o is the initial viscosity of the solution, χ^o_{pol} is the mass fraction of polymer in the initial solution, χ^∞_{sol} is the mass fraction of the solvent in the gas phase at equilibrium, ν_g is the kinematic velocity of the overlying gas, c is a constant that depends upon the Schmidt constant, D_g is the diffusivity of the overlying gas, ρ is the density of the solution, p_{sol} is the vapor pressure of the solvent, M_{sol} is the molecular weight of the solvent, R and T represent the ideal gas constant and absolute temperature, and ω is the angular speed. Eq 1 predicts that several experimental parameters, including solution concentration, polymer molecular weight, solvent volatility, and spin speed, can be used to change the film thickness. The success of Eq 1 in predicting the thickness dependence with respect to rotation rate and polymer concentration has been well documented [54,55] and we confirm these dependencies for polystyrene, as shown in Figures S1 and S2 in the Supplementary Information.

While Eq 1 does not show an explicit dependence on the molecular weight, the initial viscosity will depend on both the concentration and the molecular weight. The Mark–Houwink relationship is $\eta_o \propto M_{pol}^{\alpha}$, where the exponent α is polymer dependent and has an accepted value of $\alpha = 0.70$ for PS in THF [62]. Isolating all of the variables in Eq 1 except the molecular weight implies that h_o should scale as $\eta_o^{1/3} = (M^{\alpha}_{pol})^{1/3}$, i.e. a power law of the form $h_o = aM^{\beta}_{pol}$, where a and $\beta = \alpha/3$ are fitting parameters. Figure 1a shows the measured PS film thickness as a function of PS molecular weight, while all other experimental parameters are kept constant. As shown in Figure 1b, the best fit for the power law, a = 53 ± 20 nm and β = 0.21 ± 0.03 = α/3, giving α = 0.63 ± 0.09, in reasonable agreement with the accepted value.

To examine the solvent influence on the film thickness we chose a THF/DMF mixed solvent system. As shown in Table 1, the key solvent parameters relevant to spin-coating as expressed in Eq 1 are similar for THF and DMF, within a few per cent, except solvent vapor pressure and boiling point, which are related quantities. Other than the vapor pressure, the biggest difference in the relevant solvent parameters is the viscosity, but this difference will be negated in solution, where the polymer concentration will dominate the initial viscosity. Assuming that the vapor pressure follows Raoult's Law, and combining other parameters in Eq 1 into a single variable, the thickness can be written as $h_o = a'(\mathrm{X}_{DMF}p^o_{DMF} + \mathrm{X}_{THF}p^o_{THF})^{\frac{1}{3}}$, where X is mole fraction and p^o is the vapor pressure of the pure solvent and *a'* is an arbitrary parameter. Figure 1b shows the experimental data and the fit to the simplified equation with *a'* = 310 ± 35 nm.

Table 1. Solvent Properties [63].

Property	THF	DMF
Molecular weight (g/mol)	72.1	73.1
Density (g/cm^3)	0.888	0.945
Molar volume (cm^3/mol)	81.08	77.43
Boiling point (^{o}C)	66	153
Vapor pressure (kPa, 21 ^{o}C)	17.7	0.507
Viscosity (mPa·s, 25 ^{o}C)	0.55	0.82
Surface tension (mN/m, 20 ^{o}C)	28	35

Equation 1 gives a good description of the average thickness as shown by the data and fits in

Figure 1. However, closer examination of the films shows that the surface is not smooth so we pursued this further. Figure 2 shows the surface structures of the outer edges of PS films measured by optical profilometry as a function of solvent composition and molecular weight. When the solvent is primarily THF, there is a well-defined periodic surface morphology. When the solvent is DMF rich, the surface is rough but with no defined wave forms. A mixed solvent that is composed of 70/30 (v/v) THF/DMF overlays both of these surface structures where there is a roughness superimposed on a broad and shallow wave. This implies that to attain periodicity the solvent must be relatively volatile at the casting temperature or have a low boiling point.

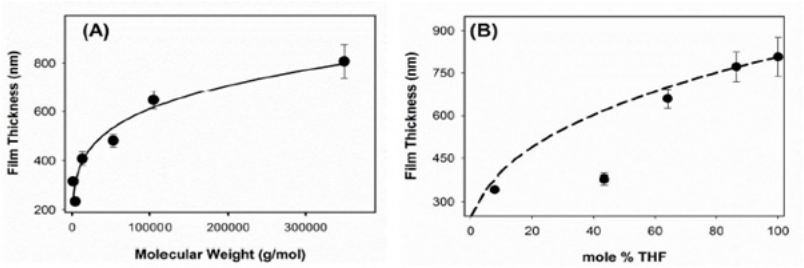

Figure 1. (a) Film thickness as a function of PS molecular weight. Films were cast using a 4% (w/v) PS solution spun at 1200 rpm. The data is fit to the equation $h_o = aM^{\beta}_{pol}$, where β = 0.21. The error bars represent a standard deviation of 9 measurements. (b) PS film thickness as a function of mole per cent THF in a THF/DMF mixed solvent. Films were cast using a 4% (w/v) solution spun at 1200 rpm. The dashed line shows a function of the form $h_o = a'(\mathrm{X}_{DMF}p^o_{DMF} + \mathrm{X}_{THF}p^o_{THF})^{\frac{1}{3}}$, where X is mole fraction and p^o is the vapor pressure of the pure solvent. The error bars show the standard deviation of at least three measurements.

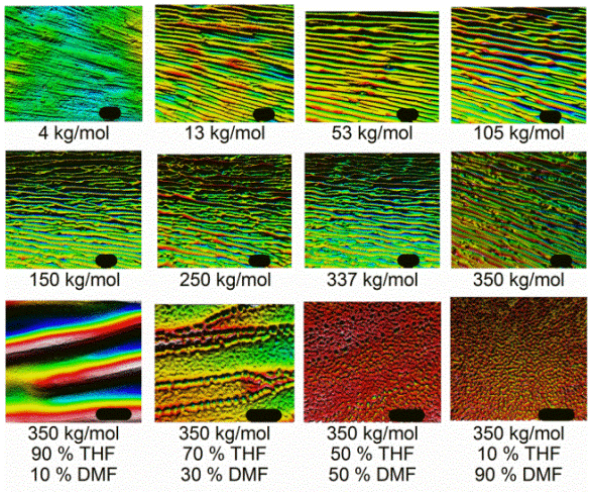

Figure 2. Surface structure of PS films cast using different molecular weights and solvent compositions. The scale bars indicate a length of 100 μm. The indicated composition percentages are v/v.

The evaporation rate of PS solutions was measured under non-spinning conditions, as shown in Figure 3. The data clearly show that the THF and DMF evaporate independently, which is expected based on the large difference in boiling points and vapor pressures. There is no evidence of azeotrope formation. Further, the evaporation rate is the same for all compositions for each component: for THF this is 0.0421 ± 0.0002 g/s and for DMF this is (1.40 ± 0.01) × 10^{-3} g/s. In the 70%THF/30%DMF solvent mixture there is a deviation from the DMF evaporation rate at long times not observed in the other data. We have no explanation for this deviation, although it may be related to a nonideality deviation from Raoult's Law. For all cases the mass change levels off at ~0.02 g, which corresponds to the remaining polymer from the 4% (w/v) solution. In the solutions that are THF rich the evaporation is more than 50% complete within ~10 s, which means that the initial structure of the surface is fixed quickly. In contrast, in DMF-rich solutions the evaporation time is much longer so the initial surface structure has more time to reconfigure. The result is that the initial periodicity is lost while the surface still has some roughness. While these evaporation results are for non-spinning conditions, the trends are expected to be the same under rotation. This is consistent with the work of Schaefer et al. [53], who showed that the length scale of polymer thin film morphology depends on the evaporation rate of the solvent. They showed that fast evaporation rates lead to kinetic controlled structures while long evaporation rates lead to thermodynamic controlled structures.

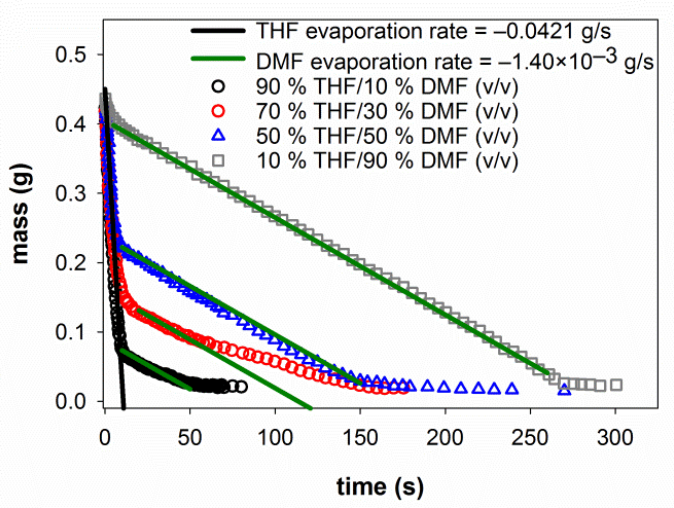

Figure 3. Evaporation of a 4% w/v solution of PS in various mixed DMF/THF compositions. The solid lines correspond to the indicated evaporation. The uncertainties in the measurements are of the size of the points.

Figure 4a shows the surface roughness as a function of solvent composition for films composed of PS with molecular weight of 350 kg/mol. As the fraction of THF in the solvent increases the surface roughness increases. This is true independent of the rotation rate. This implies that the nonuniform surface structure forms early in the coating process and only slowly relaxes into more uniform films as long as there is solvent still present. This is consistent with the static evaporation data. To further test the role of the solvent volatility, the spinning time was varied. Assuming that surface structures are randomly formed in the absence of rotation, then a short spin time will capture

the structure promoted by the initial evaporation, which should be dominated by the more volatile component of the mixed solvent。

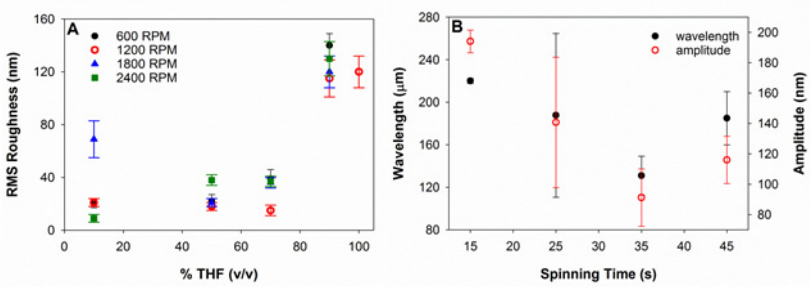

Figure 4. (a): RMS surface roughness as a function of solvent composition. (b): Amplitude (open red circles, right axis) and wavelength (filled black circles, left axis) found for PS films formed from a solvent composed of 10% DMF and 90% THF (v/v) at 1200 rpm. For both figures the molecular weight is 350 kg/mol. Raw data used for the amplitude and wavelength determinations are shown in the Supplementary Information.

Under solvent conditions with a high concentration of THF (>70% v/v) the film surface structure is periodic, as shown in Figure 2. Line scans were extracted from the surface profiles and fit to a function of the form

$$h(x) = h_o + a_o \sin\left(\frac{2\pi x}{\lambda_o}\right) \tag{2}$$

where *h(x)* is the height along the position *x* of the line scan, h_o is the average height as described in Eq 1, a_o is the amplitude of the wave, and λ_o is the wavelength. Examples of fits are shown in the Supplementary Information (Figures S3–S13). The amplitudes and wavelengths found from fitting to Eq 2 for changing the rotation rate for films created using a 4% w/v PS (molecular weight = 350 kg/mol) solution of a solvent composed of 90% THF/10% DMF (v/v) are shown in Figure 4b. All films appear dry after even the shortest spin time, but the presence or absence of solvent trapped in the films was not determined. As the residence time on the spinner increases both the wavelength and amplitude of the wrinkle structure decrease. Again, this supports the conclusion that the surface structures are formed early in the drying process.

Figure 5 shows the molecular weight dependence of the wavelengths and amplitudes of wrinkles at a constant film thickness of 310 ± 10 nm. At low molecular weights, M_n < 13 kg/mol, the periodicity is not well defined with amplitudes less than 25 nm and wavelengths in the range of 50–75 μm. Increasing M_n to the range of 53 kg/mol ⩽ M_n ⩽ 105 kg/mol, the wrinkles become more defined, the heights increase to 50–120 nm and the wavelengths increase to 90–115 μm. Finally, when M_n > 105 kg/mol the wavelengths decrease markedly, leveling out to about 75 μm. For M_n > 105 kg/mol the amplitudes also decrease but only by a small amount compared to the maximum and are approximately constant, ~75 nm, for M_n > 150 kg/mol.

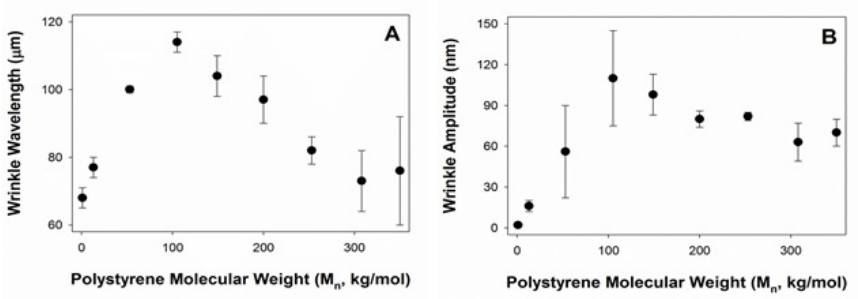

Figure 5. Average (a) Wrinkle Wavelength and (b) Wrinkle Amplitude as a function of polystyrene molecular weight. Error bars represent a standard deviation of three measurements (in some cases the standard deviations are of the size of the plotted point). The film thickness was kept constant at 310 ± 10 nm.

The changes in the wrinkle amplitude and wavelengths as a function of rotation rate are shown in Figure 6. As the spin rate increases, both the wavelength and amplitude decrease. Both of these parameters scale as $\omega^{-½}$, as shown by the solid line in Figure 6, which could imply that the surface morphology scales as the film thickness.

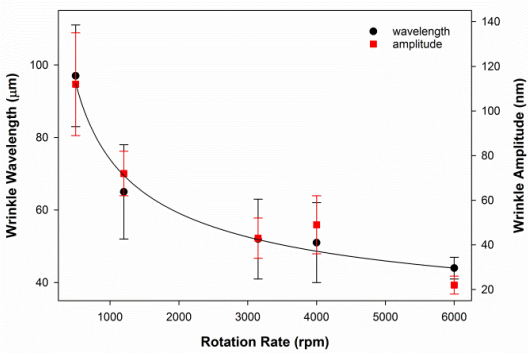

Figure 6. Average wrinkle wavelength (black dots, left axis) and amplitude (red squares, right axis) as a function of spin speed for a 2.0% (w/v) PS (M_n = 350 kg/mol) solution. Error bars represent a standard deviation of three measurements. The solid line is a fit to a function of the form $\lambda = a\omega^{-½}$, where ω is the rotation rate.

To test this conclusion, the film thickness was changed by varying the concentration of the polymer at constant rotation rate, as shown in Figure 7. Under these conditions, the wavelength and amplitude remains constant. Since the film thickness increases with increasing solution concentration (as shown in Figure S2), the data in Figure 7 demonstrate that the amplitude and wavelength of the periodic structures arise independently from the final film thickness. This then requires that the changes in observed as a function of spinning speed shown in Figure 7 are not associated with the final film thickness.

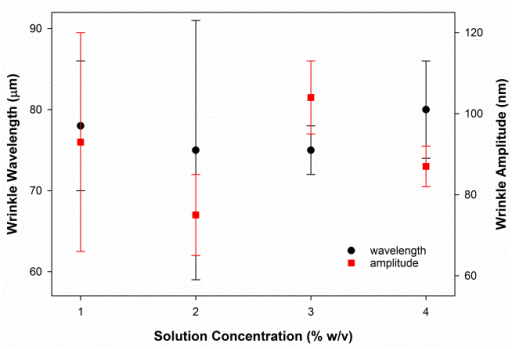

Figure 7. Average wrinkle wavelength (black dots, left axis) and amplitude (red squares, right axis) as a function of PS concentration (1200 rpm, M_n = 350 kg/mol). Error bars represent a standard deviation of three measurements.

While the average thickness of PS spin-cast films is well described by the Bornside et al. [55], model as embodied in Eq 1, this model does not account for the periodic surface morphology observed. To account for the wrinkles the model proposed by Birnie [60] is used. In the Birnie model the Marangoni effect, which is based on differential evaporation of the solvent at different spatial locations, is invoked to impose a perturbation on the initial polymer solution. The model assumes that the height of the fluid solution follows a simple sinusoidal variation:

$$H(x) = H_o + A \sin(kx) \tag{3}$$

where $H(x)$ is the fluid height at different locations x, H_o is the initial fluid height, A is the amplitude of the fluid modulation, and k is the wavenumber of the periodic perturbation. In relation to the wavelengths we have measured using Eq 2, $k = 2\pi/\lambda_o$ for the final film thickness. In order for an evaporation modulation to occur, the model [60] assumes a surface tension modulation in phase with the height modulation

$$\sigma(x) = \sigma_o + B \sin(kx) \tag{4}$$

where $\sigma(x)$ is the surface tension at location x, σ_o is the initial solution surface tension, B is the modulation amplitude of the surface tension, and the other symbols are as previously defined. The surface tension is assumed to change linearly with the fractional polymer concentration, which leads to the relation

$$C_p(x) = C_p^o + C \sin(kx) \tag{5}$$

where $C_p(x)$ is the fractional polymer concentration at location x, C_p^o is the initial fractional polymer concentration, and C is the fractional modulation of the polymer concentration. Within the Birnie [60] model the observables from our study can be found as

$$k_{max}^2 = \frac{3B}{4AH_o\sigma_o} = \frac{4\pi^2}{\lambda_o^2} \tag{6}$$

$$a_o = C_p^o H_o \left(\frac{C}{C_p^o} + \frac{A}{H_o}\right) \tag{7}$$

The values of A, B, and C may be time dependent so cannot be evaluated as independent parameters.

The terms C_p^o, σ_o, and H_o are experimentally controllable by varying the polymer concentration, solvent, and solution volume, respectively.

Qualitatively, Eqs 6 and 7 can account for the observed wavelengths and amplitudes with some caveats. The data shown in Figures 6–8 indicate that wrinkle amplitudes and wavelengths depend on the polymer molecular weight and the rotation rate but not the initial polymer concentration. The molecular weight dependence is embodied in the initial surface tension, which could account for the observed behavior. How the amplitude parameters *A*, *B*, and *C* vary with molecular weight is not known, so also could contribute to the observed dependencies. The rotation rate dependence of the surface morphology is likely related to evaporation rate changes, which will influence the composition parameter *C*. The lack of change of the observed amplitudes with initial polymer concentration is puzzling, within the context of this theory, since Eq 7 has an explicit dependence on this parameter. If Eq 7 is rewritten as $a_o = H_oC + C_p^oA$, it may be that *A* is sufficiently small that the initial concentration does not contribute significantly.

Observation of all of the data in Figures 5–7 show that λ_o and a_o show parallel dependencies on initial conditions. Combining Eqs 6 and 7 gives the following,

$$\lambda_o^2 = \frac{16\pi^2 A\sigma_o}{3BC} a_o - \frac{16\pi^2 A^2 C_p^o \sigma_o}{3BC} \tag{8}$$

which is linear for some initial conditions. Using data for a constant initial concentration and constant molecular weight, Figure 8 shows the relationship between λ_o^2 and a_o is approximately linear. Using the linear fit parameters gives the intercept/slope ratio = $-AC_p^o$ = –11 nm. The initial polymer concentration fraction, C_p^o = 0.022, allows an estimate of *A* = 500 nm. The initial fluid height can be found from the substrate surface area, 3.75 cm × 1.75 cm, and the solution volume, 500 μL, gives H_o = 760 μm. This implies that the initial amplitude variation in the polymer solution, = A/H_o, is on the order of 7×10^{-4}, which is reasonable for a small perturbation. Since the wrinkle amplitude is approximately independent of polymer concentration, ~90 nm from Figure 7, then using Eq 7 give the value for $C = 1.2 \times 10^{-4}$, which is the fractional variation of the concentration. Using Eq 6 and λ_o ~ 80 μm (from Figure 7) gives *B* = 88 mN/m, i.e. the surface tension modulation is 3 times larger than the solvent surface tension.

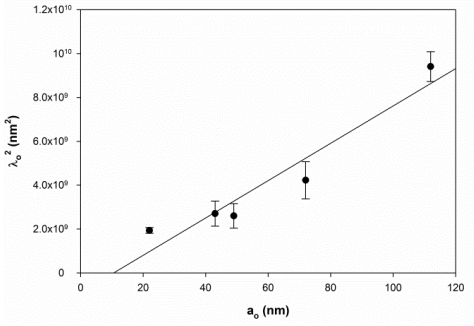

Figure 8. Wrinkle wavelength squared plotted against wrinkle amplitude for a 2.0% (w/v) PS (M_n = 350 kg/mol) solution. Error bars represent a standard deviation of three measurements. The solid line is a linear fit with slope = 8.5×10^7 nm and intercept = -9.0×10^8 nm^2 (r^2 = 0.9193).

Within the context of Birnie's model [60], this implies that a periodic surface structure is attained quickly, achieved by the initial stress at the onset of evaporation, and requires a fast evaporation rate to lock in the structure. Thus, the compositional modulation of the final dry film is primarily driven by the lateral surface tension variations of the solution as it spins. In the THF/DMF solvent system, the surface tensions of the pure solvents are similar so the changes in surface tension must be driven by concentration changes of the polymer as the solution evaporates. Further, the Birnie model [60] predicts that the time dependence of the surface tension and compositional sinusoidal amplitudes are proportional to the solvent evaporation rate. This leads to the conclusion that the amplitude of the surface wrinkle will be larger for shorter spin times. This is consistent with our data, where both the amplitude and the wavelength are larger for shorter spin times.

4. Conclusion

The surface morphology of spun cast polystyrene thin films has been studied using optical profilometry. The average film thicknesses can be accounted for by a standard model, including the role of molecular weight, rotation rate, solution concentration, and solvent composition. However, none of the PS films are smooth. Rather, for solvent compositions with fast evaporation times the surface spontaneously forms linear wrinkles that exhibit periodicity that can be described with sine waves having wavelengths on the order of tens of microns and amplitudes on the order of tens of nanometers. It was found the surface morphology changed as a function of the molecular weight of polystyrene and the rotation rate used to cast the film but was not influenced by the concentration of the polymer solution. In contrast, when the solvent evaporation rate is slow, the surfaces have reduced roughness and no periodicity, which is the classical expectation for spin coated thin films. The formation of the surface morphology was attributed to the Marangoni effect, which relies on a differential evaporation across the surface of the drying fluid. At fast evaporation rates found when the THF concentration is high, the anisotropic forces derived from the Marangoni effect prevail, leading to the kinetic structure, which are sinusoidal wrinkles. When the DMF concentration is high the evaporation rate is too low so only the isotropic rough structure is found. Quantitatively, the development of the periodic surface structure was treated as a perturbation from the average thickness, as reported in the literature, and the periodicity parameters were shown to be consistent with this interpretation. However, how this initial structure develops is still unresolved. The spatial variation in surface tension is expected to drive the final morphology, but why the perturbation should be sinusoidal is unknown. However, the underlying fundamental parameters still need to be established. The wavelengths and amplitudes of wavelike structures showed good reproducibility, which means that the perturbation parameters must be defined functions of the experimental conditions but none of these relationships are known. Both further experimental and theoretical investigations are needed to establish these relationships. The reproducibility of the periodicity is potentially useful for preparing defined surfaces. The surface morphology can be used to control the structure and spectroscopic properties of surface bound chromophores, an application that will be explored in subsequent studies.

Acknowledgments

CT thanks the Opening Foundation of Key Laboratory for Processing of Sugar Resources of

Guangxi Higher Education Institutes (2016TZYKF08) and the Scholarship Fund of Guangxi University of Science and Technology of Strengthening Foundation Program of Guangxi Higher Education Institutes in 2016 for support. This material is based upon work supported by the U.S. Department of Homeland Security, Science and Technology Directorate, Office of University Programs, under Grant Award 2013-ST-061-ED0001. The views and conclusions contained in this document are those of the authors and should not be interpreted as necessarily representing the official policies, either expressed or implied, of the U.S. Department of Homeland Security.

Conflict of interests

All authors declare no conflicts of interest in this paper.

References

1. Su J, Chen J (2017) Synthetic porous materials applied in hydrogenation reactions. *Micropor Mesopor Mat* 237: 246–259.
2. Pan L, Qiu H, Dou C, et al. (2010) Conducting polymer nanostructures: template synthesis and applications in energy storage. *Int J Mol Sci* 11: 2636–2657.
3. Share K, Westover A, Li M, et al. (2016) Surface engineering of nanomaterials for improved energy storage—A review. *Chem Eng Sci* 154: 3–19.
4. Gor GY (2014) Adsorption stress changes the elasticity of liquid argon confined in a nanopore. *Langmuir* 30: 13564–13569.
5. Ghosh J, Faller R (2008) Comparing the density of states of binary Lennard–Jones glasses in bulk and film. *J Chem Phys* 128: 124509.
6. Zhan D, Han L, Zhang J, et al. (2016) Confined chemical etching for electrochemical machining with nanoscale accuracy. *Accounts Chem Res* 49: 2596–2604.
7. Huang Z, Geyer N, Werner P, et al. (2011) Metal assisted chemical etching of silicon: A review. *Adv Mater* 23: 285–308.
8. Chen Y, Pépin A (2001) Nanofabrication: conventional and nonconventional methods. Electrophoresis 22: 187–207.
9. Fourche G (1995) An overview of the basic aspects of polymer adhesion. Part I: Fundamentals. *Polym Eng Sci* 35: 957–967.
10. Adamson AW, Gast AP (1997) Physical Chemistry of Surfaces, 6th Eds, New York: New York: Interscience publishers, 150: 180.
11. Kuwabara K, Ogino M, Motowaki S, et al. (2004) Fluorescence measurements of nanopillars fabricated by high-aspect ratio nanoprint technology. *Microelectron Eng* 73: 752–756.
12. Genet C, Ebbesen TW (2007) Light in tiny holes. Nature 445: 39–46.
13. Levitsky IA, Euler WB, Tokranova N, et al. (2007) Fluorescent polymer—porous silicon microcavity devices for explosives detection. *Appl Phys Lett* 90: 041904.
14. Lalanne P, Sauvan C, Hugonin JP (2008) Photon confinement in photonic crystal nanocavities. *Laser Photonics Rev* 2: 514–526.
15. Koo WH, Jeong SM, Araoka F, et al. (2010) Light extraction from organic light-emitting diodes enhanced by spontaneously formed buckles. *Nat Photonics* 4: 222–226.

16. Zhang L, Lang X, Hirata A, et al. (2011) Wrinkled nanoporous gold films with ultrahigh surface-enhanced raman scattering enhancement. *ACS Nano* 5: 4407–4413.
17. Hsiao YS, Charan S, Wu FY, et al. (2012) Improving the light trapping efficiency of plasmonic polymer solar cells through photon management. *J Phys Chem C* 116: 20731–20737.
18. Matoian MA, Sweetman R, Hall EC, et al. (2013) Light trapping to amplify metal enhanced fluorescence with application for sensing TNT. *J Fluoresc* 23: 877–880.
19. Zhou W, Liu R, Tang D, et al. (2013) Luminescence and local photonic confinement of single ZnSe:Mn nanostructure and the shape dependent lasing behavior. *Nanotechnology* 24: 055201.
20. Mischok A, Brückner R, Sudzius M, et al. (2014) Photonic confinement in laterally structured metal-organic microcavities. *Appl Phys Lett* 105: 051108.
21. Khang DY, Jiang H, Huang Y, et al. (2006) A stretchable form of single-crystal silicon for high-performance electronics on rubber substrates. *Science* 311: 208–212.
22. Kim DH, Ahn JH, Choi WM, et al. (2008) Stretchable and foldable silicon integrated circuits. *Science* 320: 507–511.
23. Lin PC, Yang S (2009) Mechanically switchable wetting on wrinkled elastomers with dual-scale roughness. *Soft Matter* 5: 1011–1018.
24. Ohzono T, Monobe H (2010) Morphological transformation of a liquid micropattern on dynamically tunable microwrinkles. *Langmuir* 26: 6127–6132.
25. Khare K, Zhou J, Yang S (2009) Tunable open-channel microfluidics on soft poly(dimethylsiloxane) (PDMS) substrates with sinusoidal grooves. *Langmuir* 25: 12794–12799.
26. Reiter G (1993) Unstable thin polymer films–rupture and dewetting processes. *Langmuir* 9: 1344–1351.
27. Sharma A, Reiter G (1996) Instability of thin polymer films on coated substrates: rupture, dewetting, and drop formation. *J Colloid Interf Sci* 178: 383–399.
28. Müller-Buschbaum P, Bauer E, Wunnicke O, et al. (2005) The control of thin film morphology by the interplay of dewetting, phase separation, and microphase separation. *J Phys-Condens Mat* 17: S363.
29. Wu N, Pease III LF, Russel WB (2006) Toward large-scale alignment of electrohydrodynamic patterning of thin polymer films. *Adv Funct Mater* 16: 1992–1999.
30. Schaffer E, Thurn-Albrecht T, Russel TP, et al. (2000) Electrically induced structure formation and pattern transfer. *Nature* 403: 874–877.
31. Bunz UHF (2006) Breath figures as a dynamic templating method for polymers and nanomaterials. *Adv Mater* 18: 973–989.
32. Hernandez-Guerrero M, Stenzel MH (2012) Honeycomb structures polymer films via breath figures. *Polym Chem* 3: 563–577.
33. Schaffer E, Harkema S, Blossey R, et al. (2002) Temperature gradient induced instability in polymer films. *Europhys Lett* 60: 255–261.
34. Schaffer E, Harkema S, Roerdink M, et al. (2003) Thermomechanical lithography: pattern replication using a temperature gradient driven instability. *Adv Mater* 15: 514–517.
35. Xue L, Zhang J, Han Y (2012) Phase separation induced ordered patterns in thin polymer blend films. *Prog Polym Sci* 37: 564–594.
36. Reiter G, Castelein G, Hoerner P, et al. (1999) Nanometer-scale surface patterns with long range order greated by crystallization of diblock copolymers. *Phys Rev Lett* 83: 3844–3847.

37. Lim HS, Lee SY, Lee NE, et al. (2018) Patterning of wrinkled polymer surfaces by single-step electron irradiation. *Langmuir* 34: 5290–5296.
38. Childs WR, Nuzzo RG (2002) Decal transfer microlithography: A new soft-lithographic patterning method. *J Am Chem Soc* 124: 13583–13596.
39. Fournier AC, Cumming H, McGrath KM (2010) Assembly of two- and three-dimensionally patterned silicate materials using responsive soft templates. *Dalton Trans* 39: 6524–6531.
40. Shen M (2010) Nano-structuring solid surfaces with femtosecond laser irradiations for applications. *Mod Phys Lett B* 24: 257–269.
41. Torres JM, Stafford CM, Vogt BD (2010) Impact of molecular mass on the elastic modulus of thin polystyrene films. *Polymer* 51: 4211–4217.
42. Feng C, Yi Z, Dumée LF, et al. (2015) Shrinkage induced stretchable micro-wrinkled reduced graphene oxide composite with recoverable conductivity. *Carbon* 93: 878–886.
43. Meng J, Xie J, Han X, et al. (2016) Surface wrinkling on polydopamine film. *App Surf Sci* 371: 96–101.
44. Müller-Buschbaum P, Gutmann JS, Wolkenhauer M, et al. (2001) Solvent-induced surface morphology of thin polymer films. *Macromolecules* 34: 1369–1375.
45. Xia F, Razavi B, Xu H, et al. (2002) Dependence of threshold thickness of crystallization and film morphology on film processing conditions in poly(vinylidene fluoride-trifluoroethylene) copolymer thin films. *J Appl Phys* 92: 3111–3115.
46. Pauchard L, Allain C (2003) Buckling instability induced by polymer solution drying. Europhys Lett 62: 897–903.
47. He L, Zhang L, Liang H (2008) Microdomain morphology of lamella-forming diblock copolymer confined in a thin film. *J Polym Sci Pol Phys* 47: 1–10.
48. Li B, Cao YP, Feng XQ, et al. (2012) Mechanics of morphological instabilities and surface wrinkling in soft materials: A review. *Soft Matter* 8: 5728–5745.
49. Ramanathan M, Lokitz BS, Messman JM, et al. (2013) Spontaneous wrinkling in Azlactone-based functional polymer thin films in 2D and 3D geometries for guided nanopatterning. *J Mater Chem C* 1: 2097–2101.
50. Rodríguez-Hernández J (2015) Wrinkled interfaces: taking advantage of surface instabilities to pattern polymer surfaces. *Prog Polym Sci* 42: 1–41.
51. Chapman CT, Paci JT, Lee WK, et al. (2016) Interfacial effects on nanoscale wrinkling in gold-covered polystyrene. *ACS Appl Mater Inter* 8: 24339–24344.
52. Schaefer C, Michels JJ, van der Schoot P (2016) Structuring of thin-film polymer mixtures upon solvent evaporation. *Macromolecules* 49: 6858–6870.
53. Emslie AG, Bonner FT, Peck LG (1958) Flow of a viscous liquid on a rotating disk. *J Appl Phys* 29: 858–862.
54. Bornside DE, Macosko CW, Scriven LE (1991) Spin coating of a PMMA/Chlorobenzene solution. *J Electrochem Soc* 138: 317-320.
55. Du XM, Orignac X, Almeida RM (1995) Striation-free, spin-coated sol-gel optical films. *J Am Ceram Soc* 78: 2254–2256.
56. Birnie III, DP (2001) Rational solvent selection strategies to combat striation formation during spin coating of thin films. *J Mater Res* 16: 1145–1154.
57. De Gennes PG (2002) Solvent evaporation of spin cast films: "Crust" effects. *Eur Phys J E* 7: 31–34.

58. Bassou N, Rharbi Y (2009) Role of Benard–Marangoni instabilities during solvent evaporation in polymer surface corrugations. *Langmuir* 25: 624–632.
59. Birnie III, DP (2013) A model for the drying control cosolvent selection for spin-coating uniformity: The thin film limit. *Langmuir* 29: 9072–9078.
60. Fowler PD, Ruscher C, McGraw JD, et al. (2016) Controlling Marangoni-induced instabilities in spin-cast polymer films: How to prepare uniform films. *Eur Phys J E* 39: 90.
61. Wagner HL (1985) The Mark–Houwink–Sakurada equation for the viscosity of atactic polystyrene. *J Phys Chem Ref Data* 14: 1101–1106.
62. Smallwood IM (1996) *Handbook of Organic Solvent Properties*, New York: John Wiley & Sons.

AIMS Press